Design and Microfabrication of a PVDF Acoustic Sensor

Jian Xu[a], Marcelo J. Dapino[a], Daniel Gallego Perez[b] and Derek Hansford[b]

[a] Department of Mechanical Engineering,
The Ohio State University, Columbus, OH, USA, 43210
[b] Department of Biomedical Engineering,
The Ohio State University, Columbus, OH, USA, 43210

ABSTRACT

[SMART VEHICLES WORKSHOP] This paper presents the design, theoretical analysis, microfabrication and testing of a new type of millimeter-size acoustic sensor using Polyvinylidene Fluoride (PVDF) micropillars and patterned electrodes. The sensor has the potential to achieve 100× the sensitivity of existing commercial sensors in combination with a sound pressure level (SPL) range of 35-180 dB and a frequency bandwidth of at least 100 kHz. A constrained optimization algorithm has been developed as a function of geometric parameters (sensor footprint, diameter and height of the micropillars, gap between pillar edges, and number of pillars) and electrical parameters of the sensor and conditioning amplifier. Details of the fabrication process are described. Nanoindentation tests demonstrate that the PVDF micropillar sensor exhibits piezoelectric responses under an applied voltage or strain, thus demonstrating the sensor concept. Operational amplifier circuit design and experimental setup are also described and developed.

Keywords: PVDF, microphone, sensor array, nanoindentation

1. INTRODUCTION

Existing commercial microphones are capable of either high sensitivity or broad frequency bandwidth. Typical specifications for the former category include a sensitivity of about 50 mV/Pa and a frequency range of 10 kHz, whereas transducers in the latter category exhibit a sensitivity of about 1 mV/Pa and a frequency range of 70 kHz. It is emphasized that the above sensitivities include the gain provided by the built-in amplifier placed inside of the microphone case. These microphones tend to be large, with typical geometries having a diameter of at least 12 mm. While these devices work well in many applications, there is a need for acoustic sensors capable of exhibiting high sensitivity and broad frequency bandwidth, while simultaneously having a much smaller size than the existing designs.

The availability of miniature microphones would enable new techniques for the measurement of noise-source characteristics, for example by means of extremely dense microphone arrays capable of measuring with great accuracy both pressure amplitude and direction. Such techniques will be crucial for guiding and validating the development of accurate noise prediction tools and effective suppression techniques.[1,2]

One realization of microphones is electronic stethoscopes, which are commonly used for clinical auscultation and real-time monitoring of the human respiratory system. A significant volume of research is devoted to the analysis of lung sounds based on empirical information of normal and abnormal sounds.[3,4] Electronic stethoscope arrays for measurement of breathing sounds are of great interest due to their non-invasive nature, yet the utilization of these arrays for real-time monitoring of lung sounds is confined to large sound fields in adults. The existing electronic stethoscopes are too bulky, typically 25 mm in diameter, for utilization in infants and small children.

Further author information: (Send correspondence to M.J.D)
J.X.: E-mail: xu.212@osu.edu, Telephone: 1-614-247-7480
M.J.D.: E-mail: dapino.1@osu.edu, Telephone: 1-614-688-3689
D.G.P.: E-mail: gallego-perez.2@osu.edu, Telephone: 1-614-292-9957
D.H.: E-mail: hansford.4@osu.edu, Telephone: 1-614-292-9957

Industrial and Commercial Applications of Smart Structures Technologies 2009,
edited by Benjamin K. Henderson, M. Brett McMickell, Proc. of SPIE Vol. 7290, 72900A
 · doi: 10.1117/12.817028

A variety of microphones are used in acoustic applications requiring a maximum sound pressure level (SPL) of 110-130 dB (re 20 μPa) and bandwidths of 10-20 kHz. Microphones for aeroacoustic measurements require even higher SPL in excess of 160 dB and frequency bandwidth on the order of 100 kHz, in part due to tightening regulatory constraints associated with increasing airport noise standards.

Cochlea-inspired transducers investigated by Grosh et al.[5,6] could achieve levels of miniaturization not possible with existing devices. A flexible tensioned membrane with an exponentially tapered width is employed to obtain a varying acoustic impedance, which can achieve cochlear-like frequency-position mapping. A rigid-walled duct filled with silicone oil is implemented to mimic the environment of the passive mammalian cochlea. Arnold et al.[1] designed a piezoresistive silicon microphone for aeroacoustic measurements that feature small size, high dynamic range, large frequency bandwidth, and low power consumption. The microphone consists of four dielectrically-isolated, single crystal silicon piezoresistors mounted on the top surface of a circular, tensile silicon nitride diaphragm. Several devices were investigated to characterize linearity, frequency response, drift, noise, and power. The sensors show a linear SPL up to 160 dB and a 52 dB noise floor, and consume 15 mW of power when operated at 3 V. Horowitz at al.[2] developed a micromachined piezoelectric microphone for aeroacoustic measurement applications. The microphone was fabricated by combining a lead zirconate-titanate (PZT) deposition process on a silicon-on-insulator wafer with deep reactive ion-etching. An experimental setup in a plane-wave tube was used to characterize the microphone. The device exhibits a sensitivity of 0.75 μV/Pa, dynamic range of 47.8-169 dB and resonance frequency of 50.8 kHz. Wang et al.[7] built a PZT-based microacoustic sensor that employs interdigitated electrodes and in-plane polarization instead of commonly used parallel plate-electrodes and through-thickness polarization. The sensitivity is greatly improved because of the small capacitance of the interdigitated capacitor and the large and adjustable electrode spacing, as well as the advantage of the relatively larger piezoelectric stress constant g_{33}.

The piezoelectric polymer Polyvinylidene Fluoride (PVDF), first discovered by Kawai,[8] has been widely used for sensor development in a wide range of military, industrial, and biomedical applications.[9–12] PVDF can generate voltages 10-25 times higher than piezoceramics for the same pressure input. These polymers are quite stable because they can resist moisture, most chemicals, oxidants and intense ultraviolet and nuclear radiation. PVDF is synthesized by addition polymerization of the CH2=CF2 monomer, and exhibits α, β, γ and δ phases. The α phase is the lowest energy conformation and non-polar form. The γ and δ phases are not common. The β phase form, which has a net dipole moment pointing from the electronegative fluorine to the electropositive hydrogen, produces a net dipole moment nearly normal to the polymer chain.[13] Defect groups of head to head and tail to tail are believed to be responsible for the formation of β phase and hence for the piezoelectric properties of PVDF.[14] Sensors based on PVDF film are attractive due to their high sensitivity and low cost. For example, a PVDF film pressure sensor is used for in-sleep cardiorespiratory monitoring.[15] Uncooled infrared (IR) sensors using PVDF thin film are used to detect temperature changes from low levels of incident IR radiation.[16]

Toda[17] proposed a phased-matched ultrasonic transducer based on corrugated PVDF film. In order to obtain the resonant effect of the transducer, the transducer height was chosen as one half of the acoustic wavelength. In this design, PVDF was formed into alternating concave and convex multiple curved sections that eliminates the need for clamps. Toda et al. developed a contact vibration sensor made by bonding a piezoelectric PVDF film to a curved frame structure and a rubber piece with a front contact face.[18] Pressure perpendicular to the PVDF film surface, transmitted from the rubber face, is converted to the internal circumferential stress that induces an electric charge due to the piezoelectric effect. An accelerometer mounted between the rubber face and a rigid vibration exciter plate was used to investigate the frequency response of the device, which shows the sensitivity has a flat range from 16 Hz to 3 kHz and a resonance peak at 6 kHz.

2. PROPOSED DESIGN

The primary goal of this research is to develop Polyvinylidene Fluoride (PVDF) based acoustic sensors for sound and ultrasound measurement capable of addressing the limitations in frequency bandwidth, sensitivity, and packaging of the existing designs. The target specifications of the PVDF sensors are: 1) packaged in a millimeter-sized enclosure, 2) dynamic SPL range of 35-180 dB, better than existing (35-130 dB), and 3) frequency bandwidth of 20 Hz to 100 kHz and above, possibly into the MHz range.

The voltage produced by a capacitive sensor is given by the ratio between charge and capacitance. The proposed microphone exploits the key advantages of PVDF as a sensor material by means of two key design elements aimed at increasing the charge and decreasing the effective device capacitance (Fig. 1). The first design element is a stress amplification mechanism through the area ratio between the overall surface exposed to acoustic waves and the area of the individual micropillars. Because PVDF responds to stress, this mechanism increases the amount of charge for a given pressure level. A rigid membrane placed between the micropillars and the acoustic medium ensures high mechanical coupling. The second design element is a top electrode patterned to cover only the surface of the micropillars. Excluding the capacitance of the air between pillars, the design with patterned electrodes reduces the capacitance of the sensor and hence increases the voltage generated by the sensor. The individual round electrodes above each micropillar are interconnected by means of thin conducting tabs. A flat electrode is placed underneath the array.

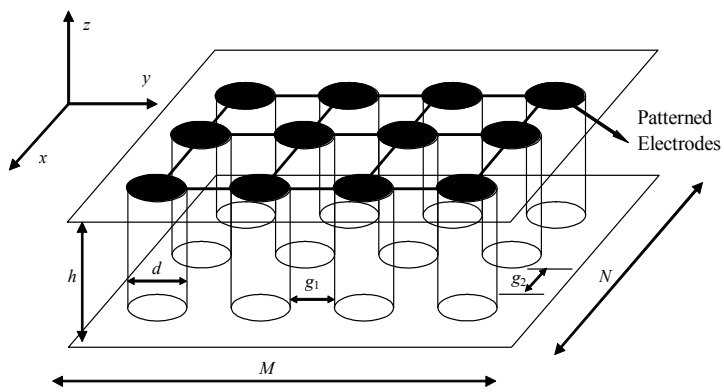

Figure 1. Schematic diagram of acoustic pressure sensor based on PVDF micropillars and patterned electrodes. A rigid membrane placed above the micropillar array acts a pressure amplifier.

3. SENSITIVITY ANALYSIS

The static sensitivity is defined as the ratio of the output voltage over the pressure acting on the PVDF material,

$$K = V_o/P. \tag{1}$$

The sensitivities of three PVDF sensor designs are compared: solid film, micropillars with full electrodes, and micropillars with patterned electrodes.

3.1 Flat PVDF film

Figure 2 shows the open circuit of a flat PVDF film sensor. The open circuit voltage developed across the film thickness is

$$V_o = -g_{33} \cdot P \cdot h, \tag{2}$$

where g_{33} is the piezoelectric stress constant in the x_3-direction, P is the applied pressure, and h is the thickness of the PVDF film. In this case, the stress induced in the material is equal to the pressure. Substitution of Eq. (2) into (1) gives the sensitivity as

$$K_1 = -g_{33} \cdot h. \tag{3}$$

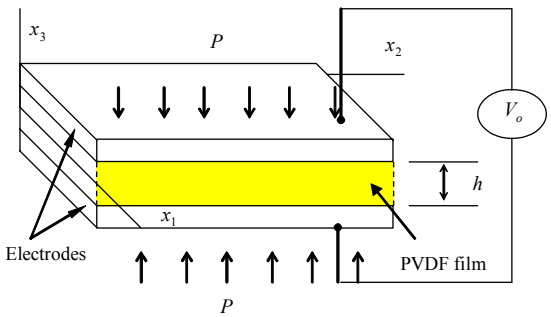

Figure 2. PVDF film open circuit.

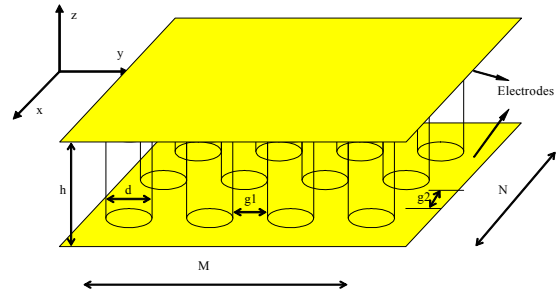

Figure 3. Schematic diagram of PVDF micropillar sensor based on full electrodes.

3.2 PVDF micropillars with full electrodes

Figure 3 illustrates the case when a continuous, flat electrode is placed atop the micropillars. The charge generated by the sensor is that generated by the micropillars,

$$Q = Q_p = C_p \cdot V_p, \tag{4}$$

where Q is the total charge collected at the electrode, Q_p is the charge generated by the micropillars, C_p is the total capacitance of the micropillars, and V_p is the voltage generated by the micropillars. The total capacitance is, by definition,

$$C_p = \varepsilon \cdot \frac{A}{h} = \varepsilon \cdot \frac{M \cdot N \cdot \pi/4 \cdot d^2}{h}, \tag{5}$$

where ε is permittivity of PVDF, M is number of pillars in the x-direction and N is number of pillars in the y-direction. According to the linear constitutive piezoelectric equations, the voltage is given by

$$V_p = -g_{33} \cdot \sigma \cdot h. \tag{6}$$

The stress on each pillar due to the application of normal pressure on the sensor surface is

$$\sigma = \frac{(d + g_1) \cdot (d + g_2)}{\pi d^2/4} \cdot P, \tag{7}$$

where d is pillar diameter, g_1 is gap between pillars in the x-direction and g_2 is the gap between pillars in the y-direction. Substitution of (7) into (6) gives

$$V_p = -g_{33} \cdot P \cdot \frac{(d + g_1) \cdot (d + g_2)}{\pi d^2/4} \cdot h. \tag{8}$$

The total capacitance is the sum of the capacitance of the micropillars and the capacitance of the air gap,

$$C_t = C_p + C_o, , \tag{9}$$

in which the air capacitance is

$$C_o = \varepsilon_o \cdot \frac{M \cdot N \cdot [(d + g_1)(d + g_2) - \pi d^2/4]}{h}. \tag{10}$$

Since the two capacitances are connected in parallel, the voltage drop is the same across the micropillars and air gap,

$$V_o = \frac{Q}{C_t}. \tag{11}$$

Combination of Eqs. (4), (5) and (8)-(11) gives the sensitivity of PVDF micropillars with full electrodes as

$$K_2 = \frac{\varepsilon_r (d+g_1)(d+g_2)}{\pi d^2/4 \cdot (\varepsilon_r - 1) + (d+g_1)(d+g_2)} \cdot (-g_{33} \cdot h), \tag{12}$$

where ε_r is the relative permittivity of PVDF. Assuming without losing generality that $g_1 = g_2 = g$, the sensitivity of the micropillar array based on full electrodes relative to the sensitivity of solid PVDF film is

$$K_{r2} = \frac{\varepsilon_r (1+g/d)^2}{\pi/4 \cdot (\varepsilon_r - 1) + (1+g/d)^2}. \tag{13}$$

The relative sensitivity of the micropillar sensor is limited by the relative permittivity of PVDF film, and the upper bound is $K_{r2} = \varepsilon_r$ as g/d goes to infinity.

3.3 PVDF micropillars with patterned electrodes

In this case both the capacitance and the charge are due solely to the micropillars, hence the sensitivity has the form

$$K_2 = \frac{(d+g_1)\cdot(d+g_2)}{\pi d^2/4} \cdot (-g_{33} \cdot h). \tag{14}$$

Assuming as before $g_1 = g_2 = g$, the sensitivity of the pillar sensors based on patterned electrodes relative to the sensitivity of PVDF film is

$$K_{r2} = \frac{(1+g/d)^2}{\pi/4}, \tag{15}$$

which increases monotonically with the ratio of the gap between pillars and the pillar diameter, g/d. The effect of the air gap between pillars is to increase the stress on the sensing material and therefore to increase the sensor's output voltage and sensitivity.

A comparison of the sensitivities of the two micropillar designs relative to that of solid PVDF film is shown in Fig. 4. The micropillar sensor with patterned electrodes theoretically has an unlimited sensitivity with increasing geometry ratio g/d (assuming $g = g_1 = g_2$).

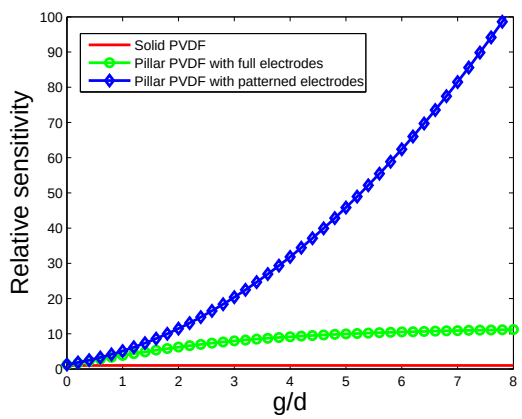

Figure 4. Relative sensitivity of the proposed PVDF micropillar sensor with patterned electrodes compared to PVDF film and fully electroded micropillars. The gaps are assumed equal ($g = g_1 = g_2$).

To simplify the design of the micropillars with patterned electrodes, we neglect the width of the connecting tabs, which is reasonable when the line width of these tabs is relatively small compared to the diameter of each pillar. The smallest tab width allowed by our current fabrication practices is about 2 microns. If the diameter of micropillars is not high enough, this factor needs to be included in the calculation of sensitivity.

4. OPTIMIZATION

Nonlinear programming (NLP) techniques are used to find a minimum or maximum of an objective function in N dimensions which satisfies arbitrary complex constraints.[19] Many algorithms have been developed for solving such problems, such as Large-Scale Optimization and Medium-Scale Optimization. The large-scale algorithm is a subspace trust region method and is based on the interior-reflective Newton method described by Coleman and Li.[20] Each iteration involves the approximate solution of a large linear system using the method of preconditioned conjugate gradients (PCG). The optimization problem can be expressed in the form

$$\begin{cases} minimize & f(x) \\ h_i(x) \leq 0 & i = 1, \ldots, m \\ g_i(x) = 0 & i = 1, \ldots, k \\ l_i \leq x_j \leq u_j & j = 1, \ldots, n \end{cases} \tag{16}$$

Here, x is an N-dimensional list of design variables; $f(x)$ is the objective function; $h_i(x)$ are inequality constraints; $g_i(x)$ are equality constraints; and $l_i \leq x_j \leq u_j$ are constraints for all design variables.

The functions $f(x)$, $h_i(x)$ and $g_i(x)$ can be any linear or nonlinear combination of the design variables. In this case, a constrained NLP optimization algorithm was developed to obtain the sensor's geometric parameters (M, N, d, g_1, g_2 and h) needed to achieve 100× the sensitivity of existing commercial sensors, dynamic range up to 180 dB, frequency bandwidth of 100 kHz, and millimeter-size footprint. The NLP optimization algorithm was integrated into Matlab.

The design variables that were optimized are M, N, d, g_1, g_2, h, and R (total input resistance of the amplifier). The design variables can be treated as independent of each other, while the dependent variables are related by the equality constraints. The total input resistance of the amplifier cannot be chosen arbitrarily as it depends on the actual specifications of available operational amplifiers, although it usually is very high. The height of the pillars is dictated by manufacturing constraints and usually takes values such as 10 μm or 20 μm. For this microacoustic sensor design, the main interest is to seek the smallest sensor which achieves a given sensitivity. Therefore, the objective function is to minimize the sensor area,

$$f(x) = M \cdot N \cdot (d + g_1) \cdot (d + g_2). \tag{17}$$

The five constraints include resonance frequency, cutoff frequency, dimensional limits in the x and y directions, sensitivity, yield strength, and buckling load. Fig. 5 to Fig. 8 respectively show pillar diameter, pillar gap, gap-to-diameter ratio, and pillar aspect ratio versus pillar height calculated through optimization based on different amplifier input resistances. Each curve represents a locus of design parameters which optimally satisfies all of the constraints. Fig. 5 shows that the calculated optimal pillar diameter monotonically increases with pillar

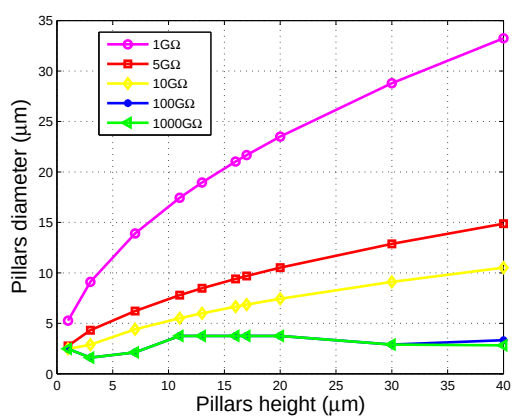

Figure 5. Optimal pillar diameter versus pillar height as a function of amplifier input resistance.

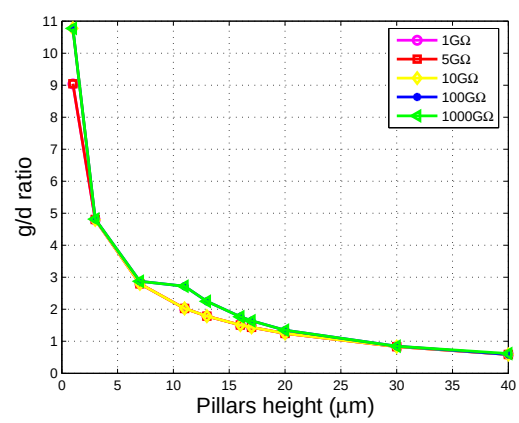

Figure 6. Optimal g/d ratio versus pillar height as a function of amplifier input resistance.

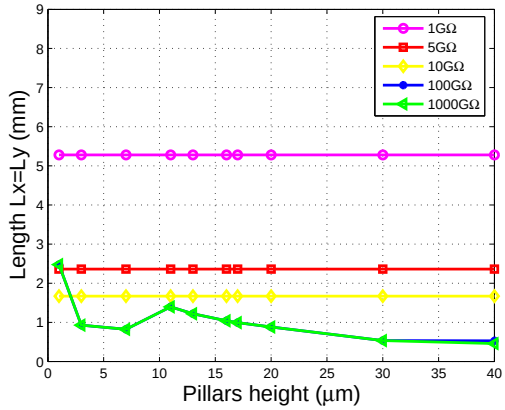

Figure 7. Optimal length versus pillar height as a function of amplifier input resistance.

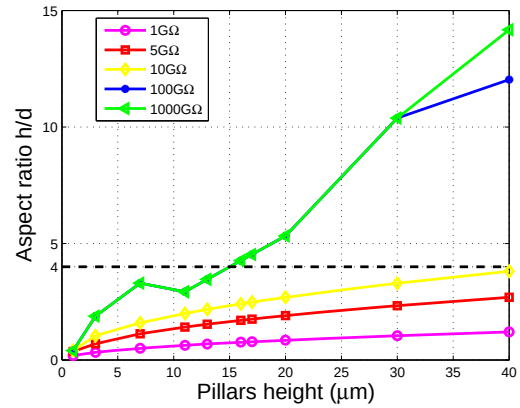

Figure 8. Optimal aspect ratio versus pillar height as a function of amplifier input resistance.

height and the increase is largest with decreasing input amplifier resistance value. Fig. 6 shows that the gap-to-diameter ratio follows the opposite trend and is nearly independent of amplifier input resistance. Fig. 7 shows that achieving an overall sensor footprint of less than 1 mm×1 mm is possible provided the amplifier input resistance is greater than 100 GΩ and the pillar height is $3 < h < 8$ μm or $h > 17$ μm. The high input resistance values tend to require aspect ratios (Fig. 8) larger than currently feasible due to manufacturing limitations ($h/d < 2$). Being able to increase the pillar height to diameter ratio to 4 or higher would enable the use of any amplifier input resistance and pillar heights of 15 μm or higher. Further details on the optimization procedure have been presented by Xu et al.[21,22]

5. MICROFABRICATION

MEMS technology has traditionally been focused on silicon based fabrication techniques. With the development of sacrificial layer micromolding (SLaM) and patterned substrate micromolding (PSM), the microfabrication of polymer microstructures is becoming increasingly promising.[23,24] We have developed a microfabrication process for realization of PVDF microstructures (Fig. 9).[25] Fig. 10 shows stamped continuous PVDF microstructures built on a flexible substrate.

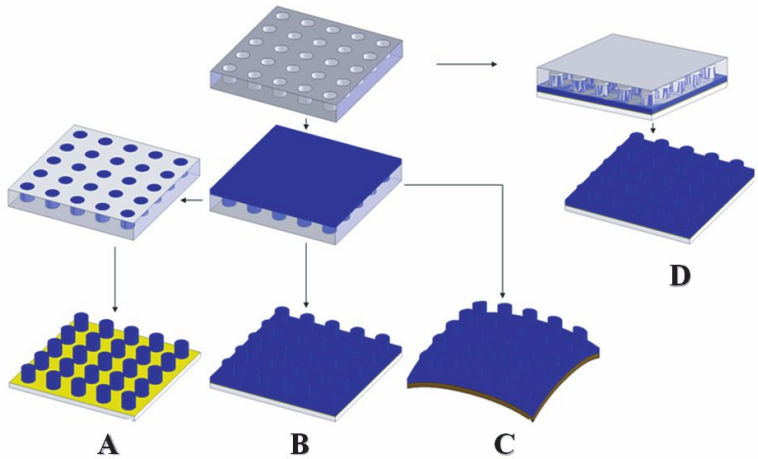

Figure 9. Schematic diagram of fabrication of PVDF microstructures: (A) Stamped discrete, (B) Stamped continuous on a rigid substrate, (C) Stamped continuous on a flexible substrate, (D) Embossed.

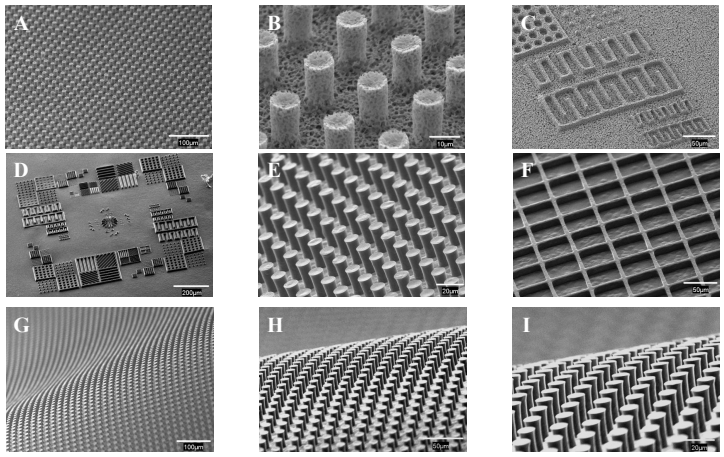

(**A-C**) Porous PVDF microstructures, (**D-I**) Annealed PVDF microstructures,
(**G-I**) SEM micrographs illustrating the pliability of the patterns.

Figure 10. Stamped continuous PVDF microstructures on a flexible substrate.

5.1 Fabrication of PVDF micropillar arrays

Previously patterned polydimethylsiloxane (PDMS) stamps molded from photolithographically fabricated masters are used in the production of individual and interconnected PVDF micropillar arrays (Fig. 11(a)). The stamps have a microwell-patterned surface with predefined diameter (d) and spacing in between edges (g). A 5-10% PVDF solution in dimethylacetamide and acetone is spin coated onto the PDMS stamps at 1000-3000 rpm for 30 seconds. The stamps are heated up to 100°C for 5 minutes to drive off the residual solvent. For interconnected micropillar arrays the PVDF is transferred onto conductive copper tape by applying about 5 psi of pressure for 5 seconds. For individual micropillar arrays the excess polymer outside the microwells (of the PDMS stamp) is selectively removed using a preheated (T=200°C) glass slide. The polymer left inside the microwells is stamped onto conductive copper tape by applying about 10 psi of pressure for 5 seconds. The copper tape serves as bottom electrode for poling and testing of the micropillars.

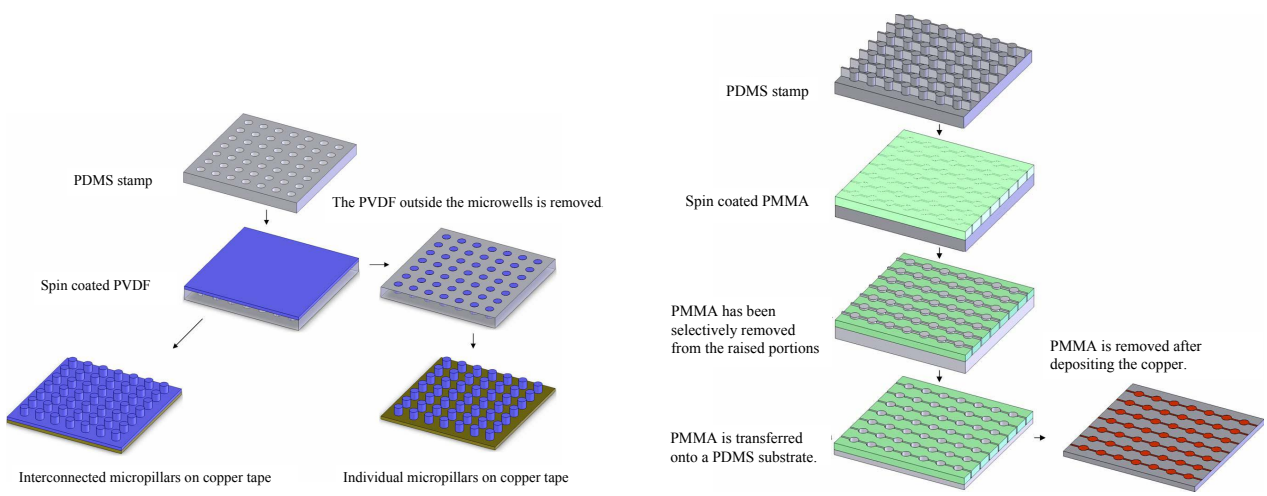

Figure 11. (a) Schematic diagram of the fabrication process. (b) Schematic diagram of the top electrode fabrication.

5.2 Fabrication of the top electrode microarray

PDMS stamps with patterned arrays of interconnected micropillars with predefined diameter, height, and spacing between edges are used in the fabrication of the top electrode (Fig. 11(b)). The micropillars are connected via 2 μm wide lines that run perpendicular to each other. A 10% polymethylmethacrylate (PMMA) solution in anisole is spin coated onto the stamps at about 3000 rpm for 1 minute. The polymer deposited on top of the micropillars and interconnecting lines is selectively removed using a preheated (T=200°C) glass slide, and the polymer left in the recessed portions of the stamp is transferred onto a flat PDMS substrate at 135°C and at around 35 psi of pressure. A thin layer (50 nm) of copper is deposited onto the PMMA-patterned PDMS substrate via electron beam evaporation. The PMMA is removed by immersing the PDMS substrate in anisole for a few minutes, which leaves a patterned microarray of copper circles and interconnection lines on the flat PDMS substrate.

5.3 Poling of the micropillar arrays

The PVDF micropillars and the copper circles of the top electrode are precisely aligned using an optical aligner (Fig. 12). The top electrode microarray is brought in contact with the micropillars upper surface, and an electric field of around 120 MV/m is applied at high temperature for a period of three hours, and then the bias is maintained for an additional hour at room temperature to sustain the dipole alignment.

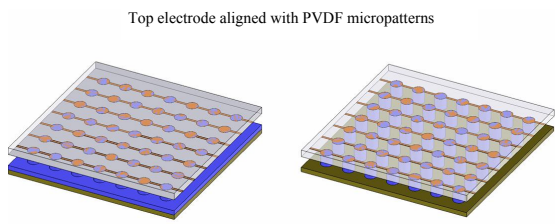

Figure 12. Top electrode is placed in direct contact with the micropillars.

6. CHARACTERIZATION EXPERIMENTS

Preliminary experiments were conducted to characterize the piezoelectric response of the PVDF micropillars. An array of 5×5 μm (5 μm spacing between edges) cylindrical pillars was chosen as a model microstructure. A gold-coated glass slide was placed on top of the micropillars (top electrode), and an electric field of ∼120 MV/m was applied across the electrodes (top positive and bottom negative) at 160°C for 3 hours, and then at room temperature for an additional hour to pole the PVDF microstructures. The direct and inverse piezoelectric responses were characterized using a Hysitron TriboIndenter nanomechanical test instrument equipped with the nanoECR package. A boron-doped diamond 14.5 μm flat punch indenter probe was used in the experiments. Load-controlled indentation testing was performed on the sample while simultaneously applying a 40 V square wave and measuring the resulting change in displacement (inverse piezoelectric effect). Fig. 13 shows a plot of displacement versus time from the 40 V square wave tests on the sample. The curves show a displacement change of approximately 5 nm (strain of 0.001) with the applied 40 Volts. Displacement-controlled nanoindentation tests were also performed on each sample and the resulting voltages were measured (direct piezoelectric effect). Fig. 14 shows plots of force and voltage versus time for the 4 μm displacement-controlled indents on the sample. A voltage of roughly 0.025 V was generated during each test. The results confirm a piezoelectric response of the PVDF micropillars under an applied voltage or strain.

7. AMPLIFIER CIRCUIT DESIGN AND EXPERIMENTAL SETUP

A PVDF microphone behaves as a capacitor, hence it generates output voltages with a high impedance level. The source impedance combined with the load resistance provided by the amplifier generates a voltage divider. As the ratio of the load resistance to the source impedance decreases, the output voltage also decreases, which

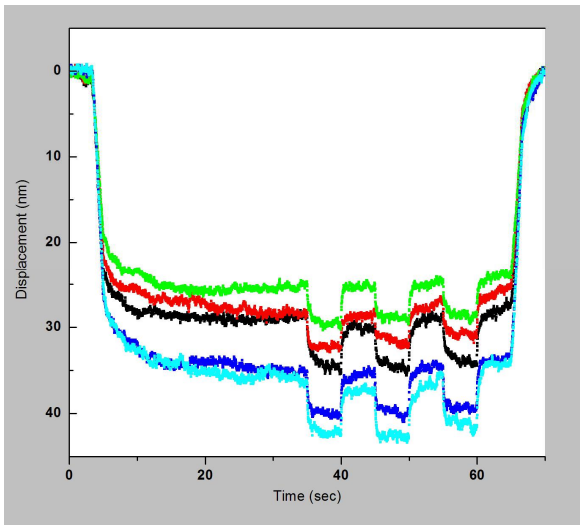

Figure 13. Plot of displacement versus time from 40 V square-wave voltage inputs.

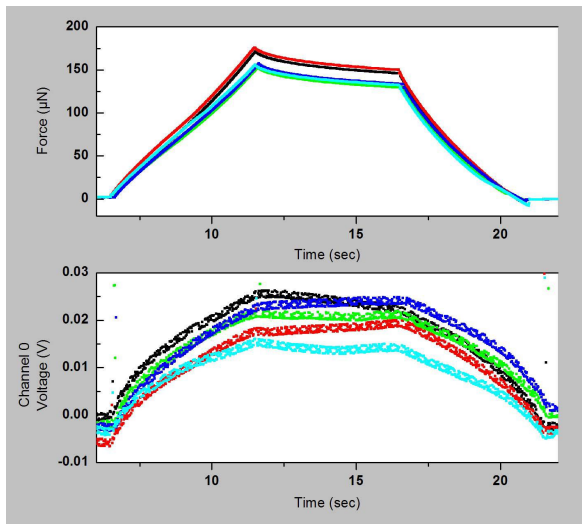

Figure 14. Plots of force and voltage versus time for the 4 μm displacement-controlled indents.

is known as the loading effect. To solve this problem, we created a buffer circuit using an operational amplifier (AD7xx, Analog Devices, Inc.) The amplifier has very high input impedance (from 2 GΩ to 300 GΩ) and small output impedance (around 10 Ω). The buffer circuit converts the high output impedance of the microphone into a low impedance which eliminates the loading effect and thus minimizes the signal loss. The amplifier circuit consists of two DC-coupled amplifiers and one high pass filter (Fig. 15). The high pass filter is utilized to filter out the drift from the dc or low frequency signal, which is found to have a relative large amplitude. The total amplification gain is the combination of the two and it could be up to 2500 or so.

The experiment shown in Fig. 16 is being developed to conduct acoustic tests under band-limit white noise excitation and to conduct sensitivity calibration tests under 250 Hz sinusoidal wave excitation. A commercial sound level meter will be used as reference. The tests will be conducted with and without enclosures. Prototype PVDF microphones based on optimized designs with various pillar dimensions and patterned electrodes were designed and a single mask including all these designs has been created and sent to the vendor. Fabrication issues such as poling and material bonding are being investigated.

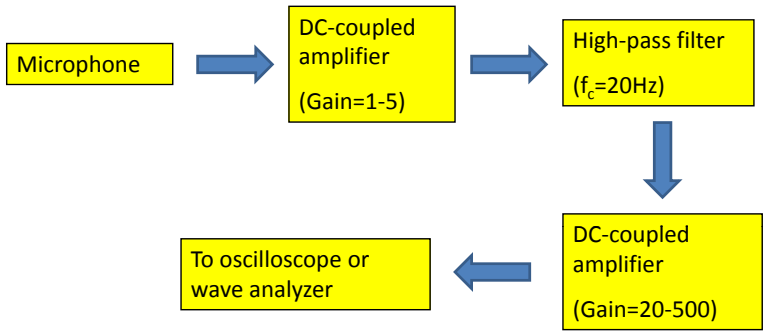

Figure 15. Schematic block diagram of the amplifier circuit design.

8. CONCLUDING REMARKS

New acoustic sensors with small size, high sensitivity, wide dynamic range and high frequency bandwidth are needed for addressing emerging requirements of many acoustic, aeroacoustic, and clinical applications. Due to their small size, high stiffness, and reduced mass, MEMS sensors can significantly improve both the temporal

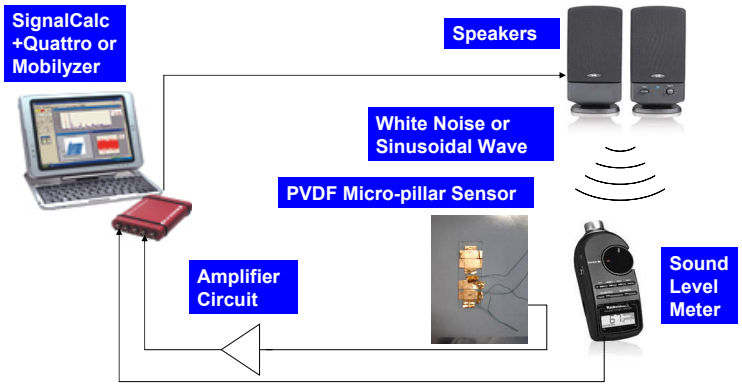

Figure 16. Schematic diagram of the experimental setup to be used for sensor benchmarking (tests will be conducted with and without enclosures).

and spatial measurement bandwidth. This article presents the design, theoretical analysis, microfabrication and characterization of a new type of millimeter-size PVDF acoustic sensor which has the potential to achieve 100× the sensitivity of existing commercial sensors in combination with a dynamic range of 180 dB and a frequency bandwidth of at least 100 kHz. Increased sensitivity is achieved through pressure amplification (created by the area ratio between the rigid surface exposed to acoustic waves and the micropillars) in combination with reduced capacitance (created by a patterned top electrode.) The superior frequency bandwidth and small footprint are made possible by the advantageous properties of PVDF and a suitable amplifier design.

The process for fabricating an acoustic sensor based on PVDF micropillars and patterned electrodes is described. In order to characterize the electromechanical properties of the sensor, a PVDF sample that consists of a uniform pattern of 5 μm pillars was manufactured and tested on a Hysitron TriboIndenter. The nanoindentation results show that the PVDF micropillar sample exhibits piezoelectric responses under an applied voltage or deformation. Future work will be focused on the fabrication and characterization of a micropillar sensor with optimal geometry. Simpler fabrication processes are being investigated.

9. ACKNOWLEGEMENTS

We are grateful to the member organizations of the Smart Vehicle Concepts Center (www.SmartVehicleCenter.org) and the National Science Foundation Industry/University Cooperative Research Centers program for supporting this work.

REFERENCES

[1] Arnold, D., Gururaj, S., Bhardwaj, S., Nishida, T., and Sheplak, M., "A piezoresitive microphone for aeroacoustic measurements," in [*2001 ASME International Mechanical Engineering Congress and Exposition*], *Proc. IMECE '01* (2001).

[2] Horowitz, S., Nishida, T., Nishida, T., and Sheplak, M., "Design and characterization of a micromachined piezoelectric microphone," in [*26th AIAA Aeroacoustics Conference*], *Proc. AIAA* (2005).

[3] Charleston-Villalobos, S., Cortes-Rubiano, S., Gonzalez-Camarena, R., Chi-Lem, G., and Aljama-Corrales, T., "Respiratory acoustic thoracic imaging (rathi): Assessing deterministic interpolation techniques," *Med. Biol. Eng. Comput.* **42**, 618–626 (2004).

[4] Murphy, R., "Patent: Method and apparatus for displaying body sounds and performing diagnosis based on body sound analysis," (September 2004).

[5] Grosh, K., Zheng, J., deBoer, E., and Nuttall, A. L., "High frequency electromotility of the cochlea," *J. Acoust. Soc. of Amer.* **115**, 2178–2184 (2004).

[6] White, R. D. and Grosh, K., "Microengineered hydrodynamical cochlear model," *Proc. of the National Acad. of Sci.* **102**, 1296–1301 (2005).

[7] Wang, Z., Wang, C., and Liu, L., "Design and analysis of pzt-based micromachined acoustic sensor with increased sensitivity," *IEEE Trans. Ultrason. Ferroelect., Freq. Contr.* **24**, 45–54 (2005).

[8] Kawai, H., "The piezoelectricity of poly (vinylidene fluoride)," *JPN. J. Appl. Phys.* **8**, 975–976 (1979).

[9] Tamura, M., Yamaguchi, T., Oyabe, T., and Yoshimi, T., "Electroacoustic transducers with piezoelectric high polymer films," *Audio Eng. Soc.* **23**, 21–26 (1975).

[10] Lerch, R. and Sesler, G. M., "Microphones with rigidly supported piezopolymer membrane," *J. Acoust. Soc. Amer* **67**, 1379–1381 (1980).

[11] Bloomfield, P., Lo, W., and Lewin, P., "Experimental study of the acoustical properties of polymers utilized to construct pvdf ultrasonic transducers and the acousto-electric properties of pvdf and p(vdf/trfe) films," *IEEE T. Ultrason. Ferr.* **47**, 1397–1405 (2000).

[12] Dias, T., Monaragala, R., and Soleimani, M., "Acoustic response of a curved active pvdf-paper/fabric speaker for active noise control of automotive interior noise," *Meas. Sci. Technol.* **18**, 1521–1532 (2007).

[13] Ramos, M., Correia, H., and Lanceros-Mendez, S., "Atomistic modelling of processes involved in poling of pvdf," *Comp. Mater. Sci.* **33**, 230–236 (2005).

[14] Dargaville, T., Celina, M., Elliott, J., Chaplya, P., Jones, G., Mowery, D., Assink, R., Clough, R., and Martin, J., "Characterization, performance and optimization of pvdf as a piezoelectric film for advanced space mirror concepts," Tech. Rep. SAND2005-6846, Sandia National Laboratories (2005).

[15] Wang, F., Tanaka, M., and Chonan, S., "Development of a pvdf piezopolymer sensor for unconstrained in-sleep cardiorespiratory monitoring," *J. Intell. Mater. Syst. and Struct.* **14**, 185–190 (2003).

[16] Fujitsuka, N., Sakata, J., Miyachi, Y., Mizuno, K., Ohtsuka, K., Taga, Y., and Tabata, O., "Monolithic pyroelectric infrared image sensor using pvdf thin film," *Sens. Actuators A* **66**, 237–243 (1998).

[17] Toda, M., "Phase-matched air ultrasonic transducers using corrugated pvdf film with half wavelength depth," *IEEE T. Ultrason. Ferr.* **48**, 1568–1574 (2001).

[18] Toda, M. and Thompson, M., "Contact-type vibration sensor using curved clamped pvdf film," *IEEE Sens. J.* **6**, 1170–1177 (2006).

[19] Gill, P., Murray, M., and Wright, M., [*Practical Optimization*], Academic Press, London (1981).

[20] Coleman, T. and Li, Y., "An interior, trust region approach for nonlinear minimization subject to bounds," *SIAM J. Optim.* **6**, 418–445 (1996).

[21] J. Xu, M.J. Dapino, D. Gallego Perez and D. Hansford, "Acoustic sensor with PVDF micro pillars and patterned electrodes," Proc. ASME Conference on Smart Materials, Adaptive Structures and Intelligent Systems, Paper #475, Ellicott City, Maryland, October 28-30, 2008.

[22] J. Xu, M.J. Dapino, D. Gallego, D. Hansford, "Microphone based on Polyvinylidene Fluoride (PVDF) micro-pillars and patterned electrodes," *Sensors and Actuators A: Physical.* In review.

[23] Lee, L., Madou, M., Koelling, K., Daunert, S., Lai, S., and Koh, C., "Design and fabrication of cd-like microfluidic platforms for diagnostics: Microfluidic functions," *Biomed. Microdevices* **3**, 245–254 (2001).

[24] Ferrell, N., Woodard, J., and Hansford, D., "Fabrication of micro- and nanoscale polymer structures by soft lithography and spin dewetting," *Biomed. Microdevices* **28**, 966–971 (2007).

[25] D. Gallego, N. Ferrell, N. Higuita, and D. Hansford, "Versatile methods for the fabrication of electroactive polyvinylidene fluoride microstructures for bioMEMS applications," *Appl. Phys. Lett.,* preprint (2008).